# A Permanently Porous Yttrium-Organic Framework Based on an Extended Tridentate Phosphine Containing Linker

*Andrey A. Bezrukov and Pascal D. C. Dietzel**

Department of Chemistry, University of Bergen, P.O. Box 7803, N-5020 Bergen

ABSTRACT

The metal-organic framework [Y(tbpp)]·*n*DMF (**1**) was synthesized from yttrium(III) nitrate and the tritopic linker 4',4''',4''''''-phosphanetriyltris(([1,1'-biphenyl]-4-carboxylic acid)) ($H_3$tbpp). The distance between the coordinating atoms of the carboxylate groups of the extended tridentate phosphine linker is more than 1.8 nm, resulting in an average pore dimension of 9 Å in the non-interpenetrated metal-organic framework. The material exhibits high thermal stability and permanent porosity after removal of guest molecules from the one-dimensional pore system. The desolvated compound adsorbs nitrogen, argon, hydrogen, and carbon dioxide. Favorable adsorption of $CO_2$ over $N_2$ is predicted using ideal adsorbed solution theory (IAST). The isosteric enthalpy of adsorption of $H_2$ and $CO_2$ of -7 kJ $mol^{-1}$ and -22 kJ $mol^{-1}$, respectively, are representative for compounds with no accessible strong host-guest binding sites, despite the bifunctional nature of the organic ligand. The absence of strong specific adsorption sites was confirmed by in-situ powder synchrotron X-ray diffraction of the reversible isobaric $CO_2$ sorption process. Analysis of the diffraction data

indicates that the $CO_2$ molecules in the pores are disordered and non-localized. Despite this, it was possible to quantify the evolution of the occupation of the pores. $CO_2$ is adsorbed at a constant rate below 320 K from 10% loading to full capacity at 195 K.

## INTRODUCTION

Metal-organic frameworks (MOFs) are coordination networks with solvent filled pores built up from inorganic and organic building blocks.[1] These porous materials show an intriguing breadth of properties within application areas such as catalysis,[2-4] sorption[5-6] and separation.[7-8] The heterogeneity of the pore surface plays a crucial role in the specific interaction between the host framework and substrate or adsorbate. An advantage of the crystalline nature of MOFs is that structural information about the interaction between host framework and guest molecule can be gained using diffraction methods.[9-10] In-situ diffraction experiments following the adsorption of gases in MOFs have been a powerful tool in elucidating site-specific adsorbate-adsorbent interaction between gas molecules and Lewis acidic or Lewis basic sites on the pore surface.[11-20]

Several organic bridging linkers derived from triphenylphosphine have been used to prepare porous coordination polymers in which metal complexes were grafted to phosphine sites,[21-28] in attempts to establish the viability of using the Lewis basic P(III) atom of the phosphine group to immobilize catalytically active systems in the MOF. It would also be interesting to study the effect of the presence of the phosphine group on the selective adsorption of environmentally relevant gases like $CO_2$. However, the adsorption properties of these materials were usually evaluated using only nitrogen physisorption.[23, 25-26, 28-30] There are only few adsorption studies relevant to gas storage and separation in these MOFs. Humphrey et al. used 4,4',4''-phosphanetriyltribenzoic acid ($H_3$tpp) to prepare the porous calcium-organic framework PCM-10.[21, 31] Its structure contains one-dimensional pores with P(III) sites

exposed on the internal surface. PCM-10 adsorbed $CO_2$ at 195 K and $H_2$ at 77 K, while the adsorption of $N_2$ and $O_2$ was negligible. Post-synthetic modification of the P(III) sites with an Au(I) complex resulted in selective adsorption of 1-hexene over *n*-hexane at 303 K and an uptake of 4.72 weight percent of $H_2$ at 77 K. We recently used the $H_3$tpp linker to synthesize the three MOFs $[Zn_3(tpp)_2(DMF)_2]\cdot n$DMF , $[Zn_3(tpp)_2(4,4'\text{-bpy})_2]\cdot n$DMF and $[Zn_3(tpp)_2(3,3'\text{-bpy})]\cdot n$DMF, all of which adsorbed $CO_2$ at 195 K.[32] A large gate effect was observed for $[Zn_3(tpp)_2(3,3'\text{-bpy})]$.

The use of extended linkers is a promising approach to obtain compounds with larger pores and a larger adsorption capacity. Here, we present the metal-organic framework $[Y(tbpp)]\cdot n$DMF (**1**) formed by reaction of the $H_3$tbpp linker ($H_3$tbpp = 4',4''',4''''''-phosphanetriyltris(([1,1'-biphenyl]-4-carboxylic acid))) and yttrium(III) nitrate (Scheme 1). The non-interpenetrated framework **1** contains infinite chains of condensed yttrium coordination polyhedra and solvent filled channels. The guest solvent molecules can be easily removed from the pores of the rigid framework, and the permanently porous compound readily adsorbs $N_2$, $H_2$, Ar, and $CO_2$. We evaluated the potential for $CO_2/N_2$ separation using ideal adsorbed solution theory (IAST). The high crystallinity of the desolvated material indicates that it should be possible to gain in-depth information about the $CO_2$ sorption process in **1**, which we investigated by in-situ powder X-ray diffraction using synchrotron radiation.

**Scheme 1.** Synthesis of compound **1**

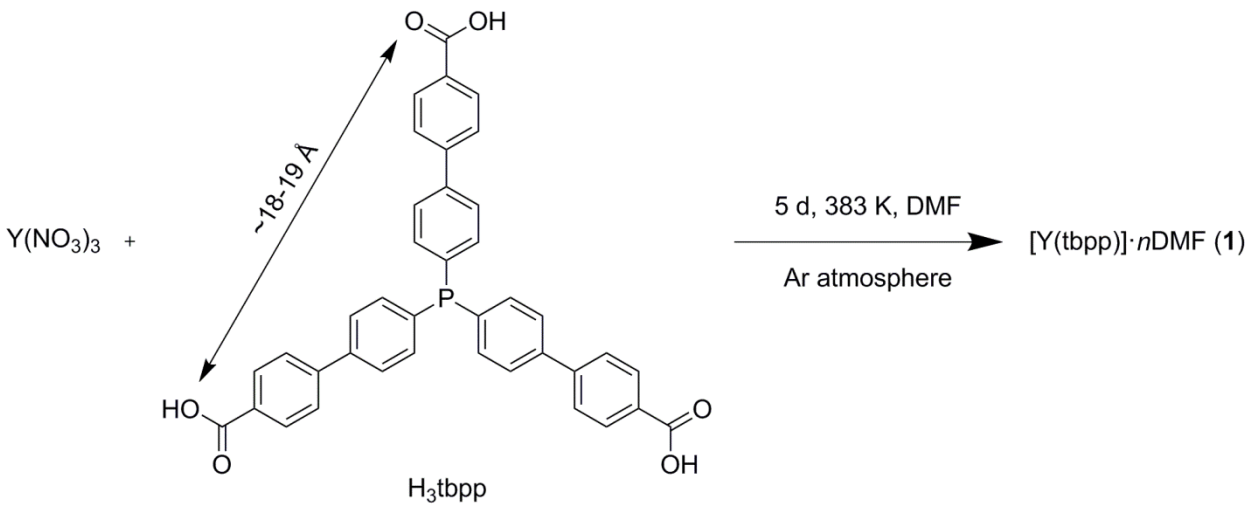


EXPERIMENTAL SECTION

***Materials.*** All chemicals, reagents and solvents were purchased from Sigma-Aldrich and used as received without further purification. In order to prevent oxidation of the P(III) in $H_3$tbpp to P(V) the synthesis was performed under inert atmosphere. Manipulations under inert atmosphere were performed using Schlenk technique or in a glove box (MBRAUN). Dimethylformamide (DMF) was deaerated using the freeze-pump-thaw procedure.

***Synthesis of the organic linker.*** 4',4''',4''''''-phosphanetriyltris(([1,1'-biphenyl]-4-carboxylic acid)) ($H_3$tbpp) was synthesized using an adapted procedure for preparation of 4,4',4''-phosphanetriyltribenzoic acid.[33-34] A detailed description of the synthetic procedure is provided in the supporting information to this article.

***Synthesis of [Y(tbpp)]·nDMF (1).*** Yttrium(III) nitrate hexahydrate (191 mg, 0.5 mmol) and $H_3$tbpp (311 mg, 0.5 mmol) were placed into a glass culture tube with screw cap (Schott, ~6 mL). The open tube was placed in a larger Schlenk flask. The atmosphere in the flask was exchanged to Ar and deaerated DMF (1 mL) was added to the mixture of solids in the tube under Ar flow. The tube was sealed with the cap under Ar flow and taken out of the larger Schlenk flask. The reaction mixture was sonicated for an hour. The tube was then placed in an

oven pre-heated to 383 K. The tube was taken out after 5 days and allowed to cool to room temperature. The solid product was filtered and washed with DMF. Yield: 355 mg (83% calculated on linker basis for [Y(tbpp)]·2DMF). Elemental analysis calcd. for $C_{39}H_{24}O_6PY \cdot 2.2C_3H_7NO \cdot 0.35H_2O$: C, 62.55; H, 4.62; N, 3.52 %. Found: C 62.54, H, 4.59, N 3.54 %.

***Single crystal structure determination.*** A suitable crystal was mounted in a minimum amount of oil in a nylon loop. Intensity data for as-synthesized **1** was collected at beamline BM01A of the Swiss-Norwegian Beamlines (SNBL) at ESRF using a custom made one-axis diffractometer equipped with a Pilatus 2M detector and an Oxford Cryostream 700 system.[35] Data processing was performed using the CrysAlisPro software.[36] Structure solution was performed using SHELXT-2014/5[37] and refinement was performed using SHELXL-2014/3.[38] The structure factor contributions from spatially disordered solvent molecules inside the pores were taken into account using SQUEEZE.[33]

**Table 1.** Crystallographic data for as-synthesized and desolvated **1**.

| Compound | As-synthesized **1** | Desolvated **1** |
|---|---|---|
| Type of X-ray diffraction experiment | Single crystal | Powder |
| Empirical formula | $C_{39}H_{24}O_6PY$ | $C_{39}H_{24}O_6PY$ |
| Formula weight | 708.46 | 708.46 |
| Temperature / K | 103 | 453 |
| Crystal system, space group | Monoclinic, *Cc* | Monoclinic, *Cc* |
| Radiation type | Synchrotron, $\lambda = 0.6973$ Å | Synchrotron, $\lambda = 0.6973$ Å |
| *a*, *b*, *c* / Å | 23.293(3), 27.463(3), 6.8852(10) | 23.2598(4), 27.5104(3), 6.96111(19) |
| α, β, γ / ° | 90, 109.649(16), 90 | 90, 109.916(2), 90 |
| *V* / Å$^3$ | 4148.0(10) | 4187.94(15) |

| | | |
|---|---|---|
| $Z$ | 4 | 4 |
| Calculated density / $Mg \cdot m^{-3}$ | 1.134 | |
| Absorption coefficient / $mm^{-1}$ | 1.48 | |
| F(000) | 1440 | |
| Theta range for data collection / ° | 2.3 to 24.5 | 1.5 to 27.0 |
| Index ranges | $-25 \leq h \leq 25$,<br>$-32 \leq k \leq 32$,<br>$-8 \leq l \leq 8$ | |
| Reflections collected | 16332 | |
| Independent reflections | 6863 [R(int) = 0.124] | |
| Absorption correction | empirical | - |
| Refinement method | Full-matrix least-squares on $F^2$ | Rietveld |
| Data, restraints, parameters | 6863, 629,424 | |
| Goodness-of-fit on $F^2$ | 0.91 | |
| $R[F^2 > 2\sigma(F^2)]$ | 0.088 | |
| w$R(F^2)$ | 0.260 | |
| Largest diff. peak and hole / $e \cdot Å^{-3}$ | 1.10 and -0.58 | |
| $R_p$ | | 0.968 % |
| $R_{wp}$ | | 1.200 % |
| $R_{exp}$ | | 0.159 % |
| $R_{Bragg}$ | | 0.551 % |
| Goodness of fit, $R_{wp}/R_{exp}$ | | 7.545 |

***Powder X-ray diffraction and isobaric $CO_2$ sorption experiment.*** As-synthesized **1** was pre-treated in a dynamic vacuum at 473 K overnight in order to remove guest solvent molecules. The desolvated sample was transferred into a glove-box and filled into a 0.5 mm glass capillary. Quartz-glass wool was placed on top of the sample in the capillary in order to reduce the risk of the sample moving within the capillary as pressure changes during the adsorption experiment. The capillary was flame sealed for transportation.

Variable temperature in-situ powder X-ray diffraction under static $CO_2$ pressure was performed at beamline BM01A of the Swiss-Norwegian Beamlines (SNBL) at ESRF. A custom sample holder was used for the experiment.[39] The glass capillary with the sample and wool inside was glued to the sample holder. The sample holder was connected to a gas dosing system, which allowed exposure of the sample to vacuum or to $CO_2$. An Oxford Cryostream 700 system was used to heat and cool the sample. It was heated at 453 K in a dynamic vacuum for 20 minutes in order to ensure the absence of guest molecules. Then, $CO_2$ was dosed at the pressure of 1 bar and the temperature was decreased from 453 K to 195 K with a ramp of 2 K $min^{-1}$. The sample was kept for 15 minutes at 195 K in order to allow the system to reach equilibrium, after which the sample was heated to 298 K with a ramp of 2 K $min^{-1}$.

Powder X-ray diffraction intensity data was collected using a custom made diffractometer equipped with a Pilatus 2M detector. 2D frames were integrated azimuthal with the *Bubble* tool.[35] Pawley profile fits of the powder diffraction patterns were performed using TOPAS 4.2. Structure of desolvated **1** was determined by Rietveld refinement using TOPAS 6.[40] The Fourier electron density difference maps were calculated from powder X-ray diffraction patterns based on a procedure described by Smeets et al.[41]

CCDC 1553721−1553722 contain the supplementary crystallographic data for as-synthesized and desolvated **1**. These data can be obtained free of charge from the Cambridge Crystallographic Data Centre via www.ccdc.cam.ac.uk/structures/.

***Thermal analysis.*** A Netzsch STA 449 F1 Jupiter was used for simultaneous thermogravimetric-differential scanning calorimetry measurements. Measurements were performed using a flow of pure Ar or $O_2$/Ar (20/80 mixture) and a heating rate of 2 K $min^{-1}$.

***Volumetric gas adsorption.*** Gas adsorption measurements were carried out on a BELSORP-max instrument. The gases used were of 99.9995 %, or higher, purity and were purchased

from Yara Praxair. As-synthesized **1** was pre-treated by heating in a dynamic vacuum at 473 K overnight. Sample was transferred into the glove-box, where sample cells were filled and transferred to the instrument under inert atmosphere using quick seals. Prior to the sorption experiment, the sample cells were again heated overnight in a dynamic vacuum at 473 K. A cross sectional area of 0.162, 0.142 and 0.195 $nm^2$ was used for $N_2$, Ar and $CO_2$ respectively, in the calculation of the specific surface area.[42] Ideal solution adsorbed theory (IAST) calculations were performed using the open-source Python package pyIAST.[43]

## RESULTS AND DISCUSSION

The presence of Lewis basic sites in the structure of MOFs frequently facilitates the selective adsorption of gas molecules like $CO_2$.[5, 44] Examples of $CO_2$ adsorption in metal-organic frameworks with uncoordinated Lewis basic P(III) sites are so far limited to frameworks based on 4,4',4''-phosphanetriyltribenzoic acid ($H_3$tpp).[21, 31-32] It is a natural progression to employ an extended derivative of $H_3$tpp in the preparation of the framework compound in the expectation that it would lead to larger pore sizes and adsorption capacities. 4',4''',4''''''-phosphanetriyltris(([1,1'-biphenyl]-4-carboxylic acid) ($H_3$tbpp) is a rigid molecule with a distance of ~18-19 Å between carboxylic acid groups, which implies potential to obtain networks with sufficiently large pore size. In cases where the organic linker is not commercially available, linker synthesis frequently becomes the reaction step determining progress in the discovery of new MOFs. Lin *et al.* recently synthesized the $H_3$tbpp linker using C–C cross-coupling reaction.[28] Herein, we used an alternative synthetic route that requires only two steps starting from commercially available reactants and avoids the use of the costly palladium based coupling agent.

We selected yttrium(III) as counter-ion for synthesis of the MOF in expectation that the hard Lewis acid $Y^{3+}$ will be exclusively coordinated by the oxygen atoms of the carboxylate

groups of the $tbpp^{3-}$ linker and not by the soft Lewis basic phosphorus atom. This synthetic strategy avoids formation of networks with metal-P coordination bonds, which have been obtained with other metal cations.[45-50] Rather, it leads to formation of a framework structure with uncoordinated P atoms.

Another challenge for the synthesis of MOFs with the $H_3tbpp$ linker is the ease of oxidation of P(III) to P(V)=O at the elevated temperatures at which the solvothermal reaction is carried out. While the oxide derivative of the $H_3tbpp$ linker does form coordination polymers, the P(V)=O group is usually coordinated to oxophilic metal atoms and participates in formation of the framework.[51] In order to avoid oxidation to the phosphine oxide and synthesize structures with the P(III) moiety, reactions including the $H_3tbpp$ ligand have to be performed under inert atmosphere and using deaerated solvents, which significantly increases the effort required for the materials discovery process.

Colourless single crystals of **1** were obtained by reaction of $Y(NO_3)_3 \cdot 6H_2O$ with $H_3tbpp$ in DMF for 5 days at 383 K under inert conditions. The trivalent metal cation and the linker anion bearing three carboxylate groups form a charge neutral framework with 1:1 composition. **1** crystallizes in the non-centrosymmetric monoclinic space group *Cc* (Table 1). Each Y atom is coordinated by nine oxygen atoms belonging to six different carboxylate groups. The inorganic secondary building unit (SBU) consists of adjacent Y atoms that are connected through $\mu$-$\eta^1$:$\eta^2$- coordinated carboxylate groups into an infinite chain of condensed Y coordination polyhedra parallel to the *c* axis (Figure 1a). The inorganic SBUs are connected by $tbpp^{3-}$ linkers into a three-dimensional non-interpenetrated coordination network. The structure has pores in the shape of rhombic channels along the *c* axis, with diagonals of approximately 7 and 10 Å (Figure 1b). The pores are filled with disordered solvent molecules in the as-synthesized compound. The solvent accessible volume amounts to 1409 $Å^3$ or 34 % of the unit cell volume (calculated using PLATON[52]), which is sufficient

space to accommodate the two DMF solvent molecules per formula unit indicated by elemental and thermal analysis.

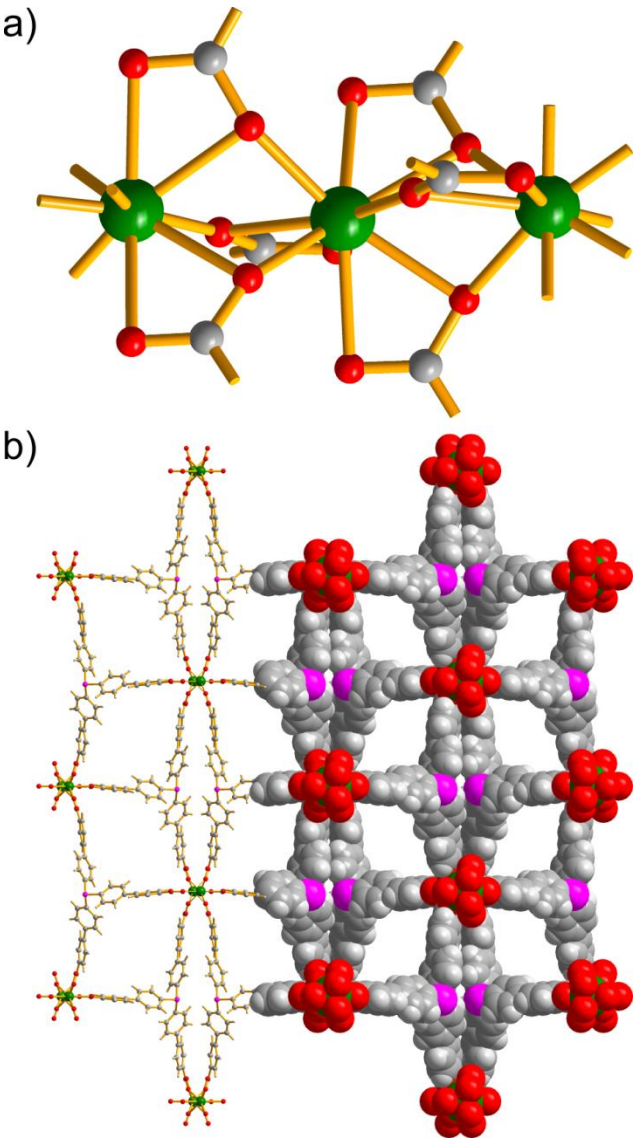


**Figure 1.** Crystal structure of **1**. a) Chain of condensed Y(III) coordination polyhedra forming the Y-based inorganic secondary building unit, b) View of the structure along [001] showing the rhombic channels (color code: Y, green; P, magenta; O, red; C, grey; H, white).

As expected, the P atom of the $H_3$tbpp linker is not coordinated to the yttrium atom in the structure of **1**, as has also been the case for other coordination networks based on tridentate phosphine linkers.[21, 28, 32, 34] Unfortunately, the non-coordinated P atom in **1** is not accessible

from the pore volume because it is pointing towards an adjacent molecule with which it forms a double wall between channels. This fact restricts the application of **1** in post-modification and as anchor for catalytically active species.

The $H_3$tbpp linker is isostructural to other tritopic linkers that were used in syntheses of coordination networks, e.g. linkers containing N,[53-66] B[67-68] or SiOH[69] instead of P as the central atom. The use of some of these tritopic linkers has led to formation of structures similar to **1**, in which three-dimensional frameworks are built from various infinite chains of condensed coordination polyhedra interconnected by the linker around one-dimensional pores parallel to the direction of the chains.[58-59, 66] The compound [Ce(L)]·1.5$H_2O$·0.5EtOH·DMF ($H_3L$ = 4',4''',4''''''-nitrilotris(([1,1'-biphenyl]-4-carboxylic acid))) (FIR-8) actually crystallizes with a framework isostructural to **1**. It is based on a nitrogen-containing linker and trivalent cerium cation and exhibits second-harmonic generation.[58]

Thermal analysis of as-synthesized **1** shows a decrease of weight of 16 % at about 440 K, corresponding to the loss of the two DMF molecules per formula unit (Figure 2). In Ar atmosphere, the loss of the solvent is followed by a pronounced plateau in the temperature range 500–770 K indicating that **1** remains stable after desolvation at elevated temperatures in inert atmosphere. In oxidizing environment ($O_2$/Ar atmosphere) the weight percent signal does not significantly drop until ~700 K. In fact, a weight increase of ~2 % is observed with a maximum at about 650 K. This weight increase corresponds to the addition of one O atom per $tbpp^{3-}$ anion and is in all likelihood due to the oxidation of P(III) to P(V)=O.

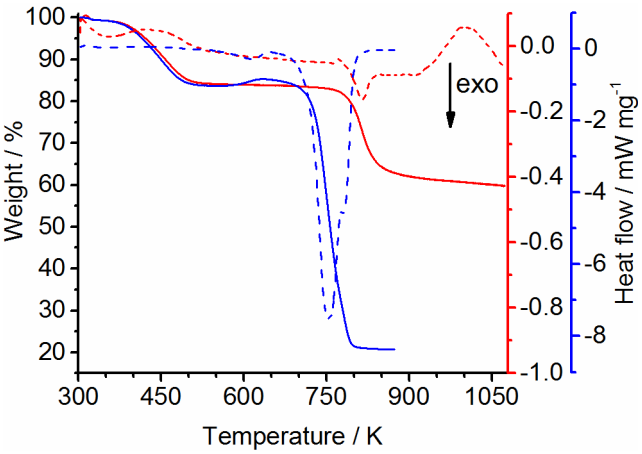


**Figure 2**. Simultaneous thermogravimetry (solid line) and differential scanning calorimetry (dashed line) of as-synthesized **1** in Ar (red) and $O_2$/Ar (20/80) atmosphere (blue).

The solvent molecules can be removed from the pores of as-synthesized **1** by treating the sample at 473 K in a dynamic vacuum overnight. The desolvated material adsorbs $N_2$, $H_2$, Ar, and $CO_2$ (Figure 3). The Langmuir and BET specific surface areas values are 915 and 781 $m^2$ $g^{-1}$ for $N_2$, 814 and 663 $m^2$ $g^{-1}$ for Ar, and 903 and 747 $m^2$ $g^{-1}$ for $CO_2$, respectively. The observed total pore volume of 0.32 $cm^3$ $g^{-1}$ (at $p/p_0$ = 0.5 for $N_2$ adsorption) corresponds well to the pore volume of 0.29 $cm^3$ $g^{-1}$ calculated for single crystal structure using PLATON.[52] A narrow pore diameter distribution with a maximum at 9 Å was found from the Ar adsorption isotherm at 87 K and NLDFT calculation with cylindrical pore model (Figure S14), corresponding well with the rhombus profile of the channel with diagonals of about 10 Å and 7 Å as determined from the single crystal structure of as-synthesized **1**.

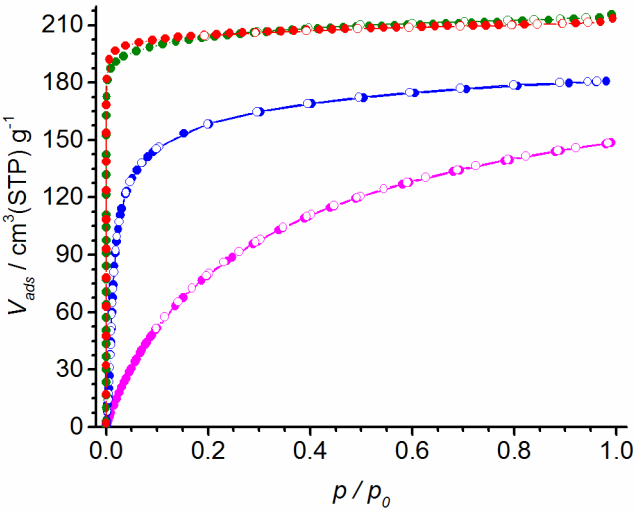


**Figure 3**. Sorption isotherms of nitrogen at 77 K (red), argon at 87 K (green), carbon dioxide at 195 K (blue) and hydrogen at 77 K (magenta) on desolvated **1**. The adsorption branch is shown as closed symbols, whilst the desorption branch is shown as open symbols. Lines are only there to guide the eye.

Desolvated **1** remains highly crystalline (Figure S7). Its crystal structure was determined by Rietveld refinement of powder X-ray diffraction data using synchrotron radiation collected at 453 K in dynamic vacuum (Figure 4a). The structure of desolvated **1** differs from the single crystal structure of as-synthesized **1** only by minor conformational changes (Figure S9), which confirms that **1** is a rigid (2nd generation) permanently porous MOF.[70] The absence of significant electron density in the pores in the Fourier difference map confirms the successful removal of solvent guest molecules (Figure 5a).

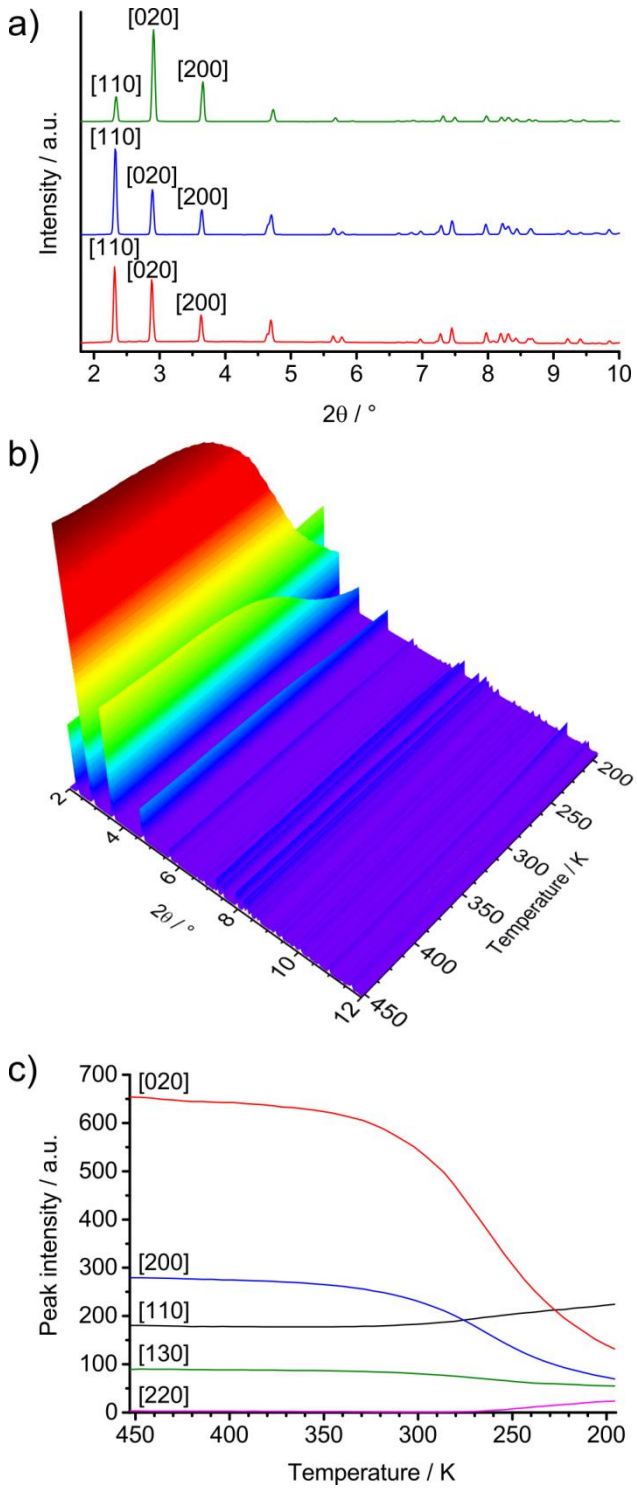


**Figure 4.** a) Powder X-ray diffraction patterns of desolvated **1** at 453 K in a dynamic vacuum (green), **1** loaded with $CO_2$ at 1 bar and 195 K (blue) and as-synthesized **1** at 298 K (red) measured using synchrotron radiation (λ = 0.6973 Å), plotted with normalized intensities. Note that the absolute intensity of the [110] reflection changes very little compared to the

[200] and [020] reflections, see c), b) 3D plot of the variable temperature powder X-ray diffraction patterns measured using synchrotron radiation (λ = 0.6973 Å) for adsorption of $CO_2$ on desolvated **1** under isobaric conditions ($p$ = 1 bar), c) Intensity change of the first 5 reflections as a function of temperature, as derived from the Pawley profile fits during $CO_2$ adsorption on desolvated **1** under isobaric conditions ($p$ = 1 bar).

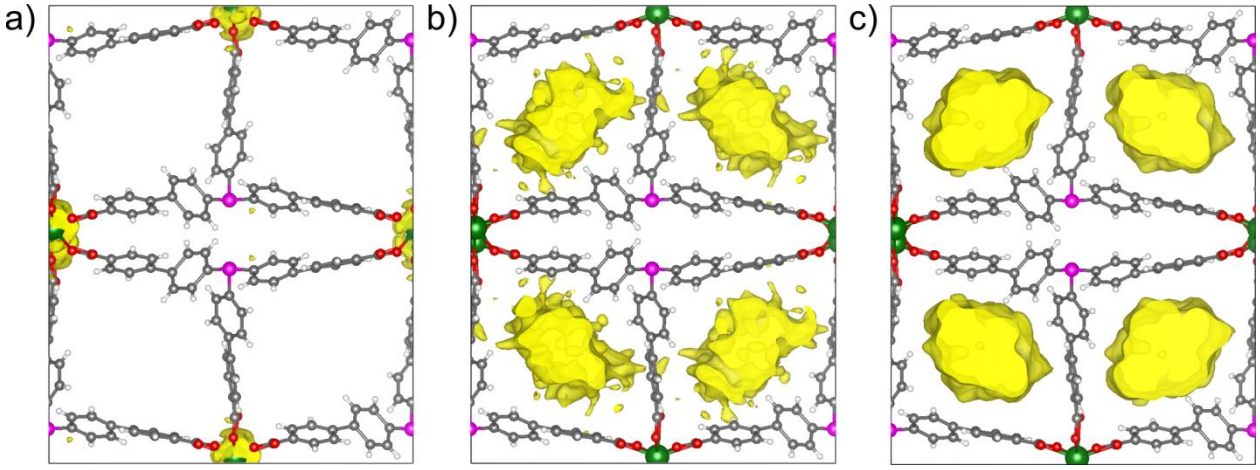


**Figure 5.** Fourier electron density difference maps ($F_{obs} - F_{calc}$) with positive electron density shown with isosurfaces at 50 % of $F_{max}$, generated from a) The Rietveld refinement of desolvated **1** at 453 K in vacuum. b) The structural model obtained from Rietveld refinement of desolvated **1** and powder X-ray diffraction pattern at 270 K at 1 bar $CO_2$. c) The structural model obtained from Rietveld refinement of desolvated **1** and powder X-ray diffraction pattern at 195 K at 1 bar $CO_2$. View along [001] (color code: Y, green; P, magenta; O, red; C, grey; H, white; electron density, yellow).

We subsequently exposed this desolvated sample to $CO_2$ under isobaric conditions ($p$ = 1 bar) and collected in-situ powder X-ray diffraction data while cooling down and heating up the sample in an attempt to follow the adsorption and desorption process and gain structural information about dynamic processes occurring in **1**.[20] Upon exposure to $CO_2$ and continuous

decrease of the temperature from 453 K to 195 K, increasing amounts of $CO_2$ are adsorbed in **1**, which is reflected by continuous changes of relative intensities of the reflections in the powder X-ray diffraction patterns (Figure 4b). There is no significant change of the lattice parameters during adsorption which corroborates the rigidity of the framework during the adsorption process. The relative change is 0.4 % for *a*, 0.5 % for *b*, and 0.7 % for *c* in the temperature range 453-195 K (Figure 6). The powder pattern at 195 K, at which the pores are fully filled with $CO_2$, exhibits a similar distribution of relative intensities as as-synthesized **1** with solvent molecules in the pores (Figure 4a). The intensities of the [020] and [200] reflections relative to the [110] reflection are the most affected by the pore content of the framework, whether it is solvent or adsorbed $CO_2$ molecules (Figure 4b and c).

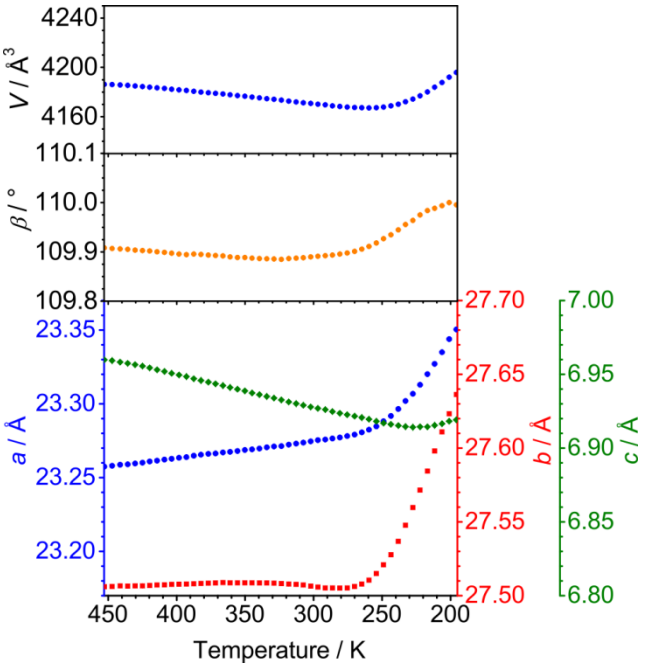


**Figure 6.** Lattice parameters in dependence of temperature during $CO_2$ adsorption on desolvated **1**.

Regrettably, our attempts to localize the $CO_2$ molecules in the pore of the fully loaded structure at 195 K did not succeed despite the excellent quality of the diffraction data and clear differences in the relative intensity distribution of the desolvated and $CO_2$ loaded

compound. The most likely explanation for the failure to find definite locations for the $CO_2$ molecules is that the individual $CO_2$ molecules are disordered instead of on well-defined positions in the pore. This interpretation is corroborated by the Fourier electron density difference maps obtained for two exemplary temperatures, representing different $CO_2$ occupancies (Figure 5b-c). There is significant electron density located in the pores at both 270 K and 195 K, confirming that **1** adsorbed increasing amounts of $CO_2$ as the temperature was decreased under isobaric pressure. The electron cloud is relatively diffuse in the pores at 270 K (Figure 5b). At 195 K (Figure 5c), at which the amount of adsorbed $CO_2$ is maximal, the electron density is distributed inside the pore channel following the shape of the Connolly surface more closely, thus filling the pore more completely than the lower density at the higher temperature. In neither map are there isolated maximums of electron density that indicate the presence of well localized individual $CO_2$ molecules.

Even though the determination of well-defined host-guest structures was not possible, we were able to obtain a more detailed picture of the sorption process by quantification of the number of $CO_2$ molecules that are adsorbed in the pores at variable temperature. The electron density in the pores due to the adsorbed disordered $CO_2$ can be accounted for using the SQUEEZE routine in PLATON[52] (Figure 7), which was performed on *hkl* intensity sets obtained from Rietveld refinements using the fixed structural model of desolvated **1**. The calculated $CO_2$ uptake continuously changes over time, reflecting the smooth change of intensities in the powder X-ray diffraction patterns (Figure 4b-c). Upon cooling from 453 K to 320 K, the uptake changes from 3 % to 10 %. Below ~320 K, it increases faster and reaches 100 % at 195 K with an approximately constant slope. The $CO_2$ uptake decreases again with a similar slope upon heating showing the easy reversibility of the adsorption and desorption processes, neither of which appears to be kinetically hindered. The numbers of adsorbed $CO_2$

molecules adsorbed at 278, 288 and 298 K normalized to the maximum uptake at 195 K correspond perfectly for measurements at isobaric and isothermal condition (Figure S12).

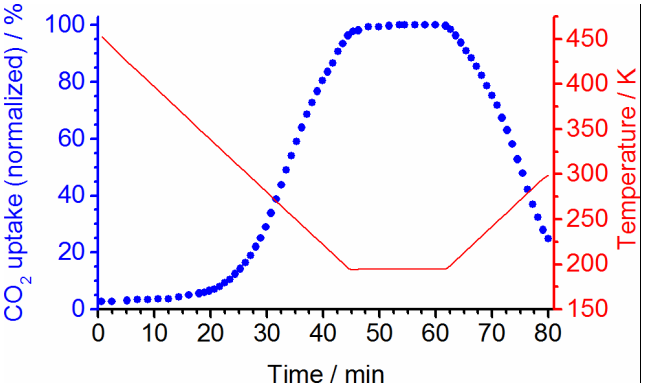


**Figure 7.** $CO_2$ uptake inside the pore of **1** (blue) and temperature as function of time (red) during the adsorption and desorption of $CO_2$ at isobaric conditions ($p$ = 1 bar), expressed in the form of number of electrons in the pores calculated using the SQUEEZE routine in PLATON (normalized, see Figure S10, S12 and accompanying explanation).

Volumetric gas adsorption experiments (Figure S13) were used to quantify the strength of the interaction between framework and adsorptive. The isosteric enthalpy of adsorption of $CO_2$ in the temperature range 278–298 K is about –22 kJ $mol^{-1}$ (Figure 8a), which is in the range usually found for MOFs without preferred strong adsorption sites such as open-metal sites[11, 16, 71-78] or available Lewis basic sites.[78-88] Hydrogen adsorption at 77 and 87 K achieved higher coverage of the internal surface than $CO_2$ adsorption close to room temperature. The isosteric enthalpy of adsorption of hydrogen does not change significantly as the $H_2$ uptake increases to 3 molecules per formula unit (Figure 8a), indicating that different adsorption sites are energetically similar. At approx. –7 kJ $mol^{-1}$, it is again typical for MOFs without strong adsorption sites.

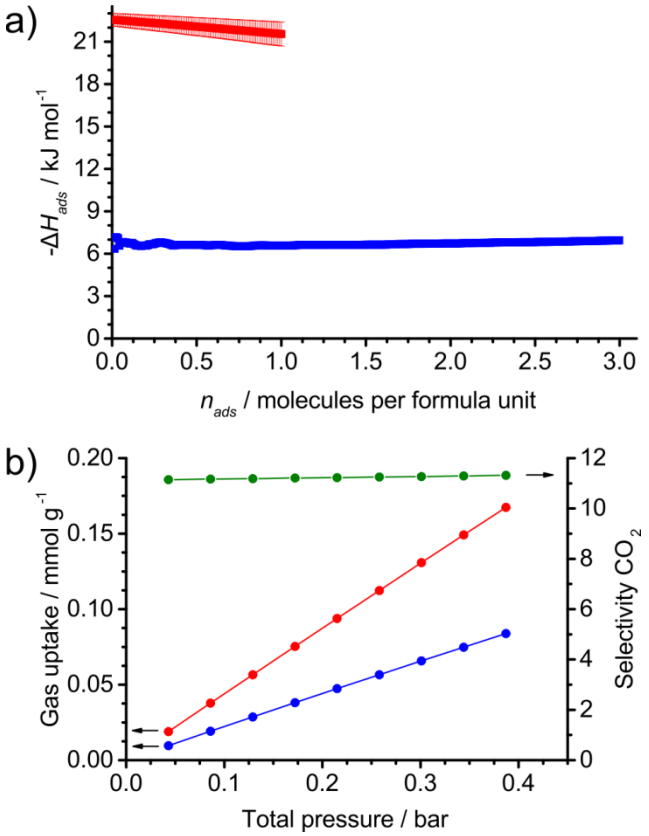


**Figure 8.** a) Isosteric enthalpy of adsorption of carbon dioxide (red) calculated from isotherms at 278, 288 and 298 K and of hydrogen (blue) calculated from isotherms at 77 and 87 K, b) IAST calculation for binary mixture of $CO_2$ (15 %) and $N_2$ (85 %) at 278 K: predicted adsorption of $CO_2$ (red) and $N_2$ (blue) and selectivity of adsorption of $CO_2$ over $N_2$ (green).

The rigidity of the framework **1** during the adsorption process allowed us to apply ideal solution adsorbed theory (IAST)[89] calculations to predict mixed-gas adsorption isotherms (Figure 8b) from pure-gas isotherms of $CO_2$ and $N_2$ (Figure S15). The IAST calculations were performed for a binary mixture of 15 % $CO_2$ and 85 % $N_2$, simulating the content of $CO_2$ in flue gas.[90-91] The predicted adsorption selectivity of $CO_2$ over $N_2$ is about 11 at 278 K, what is lower than $CO_2/N_2$ selectivity numbers predicted with IAST for MOFs with strong adsorption sites.[77, 86, 92-96] Still, the selectivity value demonstrates that even in the absence of open metal

sites or accessible Lewis basic sites in the structure, desolvated **1** favors the adsorption of $CO_2$ over $N_2$.

## CONCLUSION

We have demonstrated that the extended tridentate phosphine linker can be used to prepare MOFs with permanent porosity, high thermal stability and large pore sizes. The rigid non-interpenetrated porous metal-organic framework **1** is permanently porous and remains crystalline after solvent removal with rhombus-shaped channels with an average pore size ~9 Å. It adsorbs $N_2$, Ar, $H_2$ and $CO_2$. The $CO_2$ sorption process was also monitored using variable temperature powder X-ray diffraction at static pressure, from which the amount of adsorbed $CO_2$ could be estimated. IAST calculations predict that **1** adsorbs $CO_2$ selectively over $N_2$.

## ASSOCIATED CONTENT

**Supporting Information**.

The following files are available free of charge.

Linker synthesis procedure, NMR spectra, powder X-ray diffraction analysis details including Rietveld refinement details, volumetric gas sorption isotherms; pore size distribution, isosteric enthalpy of adsorption and IAST calculations details (PDF)

## AUTHOR INFORMATION

**Corresponding Author**

* E-mail: pascal.dietzel@uib.no.

**Funding Sources**

Research Council of Norway through grant ISP-KJEMI 209339 and SYNKNOYT 247734.

**Notes**

The authors declare no competing financial interests.

ACKNOWLEDGMENT

This work was supported by the Research Council of Norway (ISP-KJEMI 209339, SYNKNOYT 247734). We thank Frank Mohn AS for providing liquid Ar for adsorption measurements and Dr. D. Chernyshov and Dr. I. Dovgaliuk for assistance with measurements at the Swiss-Norwegian Beamlines at the ESRF.

ABBREVIATIONS

DMF, Dimethylformamide.

REFERENCES

(1) Batten Stuart, R.; Champness Neil, R.; Chen, X.-M.; Garcia-Martinez, J.; Kitagawa, S.; Öhrström, L.; O'Keeffe, M.; Paik Suh, M.; Reedijk, J. Terminology of metal–organic frameworks and coordination polymers (IUPAC Recommendations 2013). *Pure Appl. Chem.* **2013**, *85*, 1715.

(2) Corma, A.; García, H.; Llabrés i Xamena, F. X. Engineering Metal Organic Frameworks for Heterogeneous Catalysis. *Chem. Rev.* **2010**, *110*, 4606-4655.

(3) Yoon, M.; Srirambalaji, R.; Kim, K. Homochiral Metal–Organic Frameworks for Asymmetric Heterogeneous Catalysis. *Chem. Rev.* **2012**, *112*, 1196-1231.

(4) Lee, J.; Farha, O. K.; Roberts, J.; Scheidt, K. A.; Nguyen, S. T.; Hupp, J. T. Metal-organic framework materials as catalysts. *Chem. Soc. Rev.* **2009**, *38*, 1450-1459.

(5) Sumida, K.; Rogow, D. L.; Mason, J. A.; McDonald, T. M.; Bloch, E. D.; Herm, Z. R.; Bae, T.-H.; Long, J. R. Carbon Dioxide Capture in Metal–Organic Frameworks. *Chem. Rev.* **2012**, *112*, 724-781.

(6) Murray, L. J.; Dinca, M.; Long, J. R. Hydrogen storage in metal-organic frameworks. *Chem. Soc. Rev.* **2009**, *38*, 1294-1314.

(7) Li, J.-R.; Sculley, J.; Zhou, H.-C. Metal–Organic Frameworks for Separations. *Chem. Rev.* **2012**, *112*, 869-932.

(8) Li, J.-R.; Kuppler, R. J.; Zhou, H.-C. Selective gas adsorption and separation in metal-organic frameworks. *Chem. Soc. Rev.* **2009**, *38*, 1477-1504.

(9) Carrington, E. J.; Vitorica-Yrezabal, I. J.; Brammer, L. Crystallographic studies of gas sorption in metal-organic frameworks. *Acta Crystallogr., Sect. B* **2014**, *70*, 404-422.

(10) Easun, T. L.; Moreau, F.; Yan, Y.; Yang, S.; Schroder, M. Structural and dynamic studies of substrate binding in porous metal-organic frameworks. *Chem. Soc. Rev.* **2017**, *46*, 239-274.

(11) Dietzel, P. D. C.; Johnsen, R. E.; Fjellvag, H.; Bordiga, S.; Groppo, E.; Chavan, S.; Blom, R. Adsorption properties and structure of CO2 adsorbed on open coordination sites of metal-organic framework $Ni_2$(dhtp) from gas adsorption, IR spectroscopy and X-ray diffraction. *Chem. Commun.* **2008**, 5125-5127.

(12) McKinlay, A. C.; Xiao, B.; Wragg, D. S.; Wheatley, P. S.; Megson, I. L.; Morris, R. E. Exceptional Behavior over the Whole Adsorption−Storage−Delivery Cycle for NO in Porous Metal Organic Frameworks. *J. Am. Chem. Soc.* **2008**, *130*, 10440-10444.

(13) Zhang, J.-P.; Chen, X.-M. Optimized Acetylene/Carbon Dioxide Sorption in a Dynamic Porous Crystal. *J. Am. Chem. Soc.* **2009**, *131*, 5516-5521.

(14) Getzschmann, J.; Senkovska, I.; Wallacher, D.; Tovar, M.; Fairen-Jimenez, D.; Düren, T.; van Baten, J. M.; Krishna, R.; Kaskel, S. Methane storage mechanism in the metal-organic framework $Cu_3(btc)_2$: An in situ neutron diffraction study. *Microporous Mesoporous Mater.* **2010**, *136*, 50-58.

(15) Vaidhyanathan, R.; Iremonger, S. S.; Shimizu, G. K. H.; Boyd, P. G.; Alavi, S.; Woo, T. K. Direct Observation and Quantification of $CO_2$ Binding Within an Amine-Functionalized Nanoporous Solid. *Science* **2010**, *330*, 650-653.

(16) Zhou, D.-D.; He, C.-T.; Liao, P.-Q.; Xue, W.; Zhang, W.-X.; Zhou, H.-L.; Zhang, J.-P.; Chen, X.-M. A flexible porous Cu(II) bis-imidazolate framework with ultrahigh concentration of active sites for efficient and recyclable $CO_2$ capture. *Chem. Commun.* **2013**, *49*, 11728-11730.

(17) Peterson, V. K.; Southon, P. D.; Halder, G. J.; Price, D. J.; Bevitt, J. J.; Kepert, C. J. Guest Adsorption in the Nanoporous Metal–Organic Framework $Cu_3$(1,3,5-Benzenetricarboxylate)$_2$: Combined In Situ X-ray Diffraction and Vapor Sorption. *Chem. Mater.* **2014**, *26*, 4712-4723.

(18) McDonald, T. M.; Mason, J. A.; Kong, X.; Bloch, E. D.; Gygi, D.; Dani, A.; Crocella, V.; Giordanino, F.; Odoh, S. O.; Drisdell, W. S.; Vlaisavljevich, B.; Dzubak, A. L.; Poloni, R.; Schnell, S. K.; Planas, N.; Lee, K.; Pascal, T.; Wan, L. F.; Prendergast, D.; Neaton, J. B.; Smit, B.; Kortright, J. B.; Gagliardi, L.; Bordiga, S.; Reimer, J. A.; Long, J. R. Cooperative insertion of $CO_2$ in diamine-appended metal-organic frameworks. *Nature* **2015**, *519*, 303-308.

(19) Gonzalez, M. I.; Mason, J. A.; Bloch, E. D.; Teat, S. J.; Gagnon, K. J.; Morrison, G. Y.; Queen, W. L.; Long, J. R. Structural characterization of framework-gas interactions in the metal-organic framework $Co_2$(dobdc) by in situ single-crystal X-ray diffraction. *Chem. Sci.* **2017**, *8*, 4387-4398.

(20) Pato-Doldán, B.; Rosnes, M. H.; Dietzel, P. D. C. An In-Depth Structural Study of the Carbon Dioxide Adsorption Process in the Porous Metal–Organic Frameworks CPO-27-M. *ChemSusChem* **2017**, *10*, 1710-1719.

(21) Nunez, A. J.; Shear, L. N.; Dahal, N.; Ibarra, I. A.; Yoon, J.; Hwang, Y. K.; Chang, J.-S.; Humphrey, S. M. A coordination polymer of ($Ph_3$P)AuCl prepared by post-synthetic modification and its application in 1-hexene/n-hexane separation. *Chem. Commun.* **2011**, *47*, 11855-11857.

(22) Bohnsack, A. M.; Ibarra, I. A.; Bakhmutov, V. I.; Lynch, V. M.; Humphrey, S. M. Rational Design of Porous Coordination Polymers Based on Bis(phosphine)$MCl_2$ Complexes That Exhibit High-Temperature H2 Sorption and Chemical Reactivity. *J. Am. Chem. Soc.* **2013**, *135*, 16038-16041.

(23) Václavík, J.; Servalli, M.; Lothschütz, C.; Szlachetko, J.; Ranocchiari, M.; van Bokhoven, J. A. AuI Catalysis on a Coordination Polymer: A Solid Porous Ligand with Free Phosphine Sites. *ChemCatChem* **2013**, *5*, 692-696.

(24) Falkowski, J. M.; Sawano, T.; Zhang, T.; Tsun, G.; Chen, Y.; Lockard, J. V.; Lin, W. Privileged Phosphine-Based Metal–Organic Frameworks for Broad-Scope Asymmetric Catalysis. *J. Am. Chem. Soc.* **2014**, *136*, 5213-5216.

(25) Xu, X.; Rummelt, S. M.; Morel, F. L.; Ranocchiari, M.; van Bokhoven, J. A. Selective Catalytic Behavior of a Phosphine-Tagged Metal-Organic Framework Organocatalyst. *Chem. - Eur. J.* **2014**, *20*, 15467-15472.

(26) Redondo, A. B.; Morel, F. L.; Ranocchiari, M.; van Bokhoven, J. A. Functionalized Ruthenium-Phosphine Metal-Organic Framework for Continuous Vapor-Phase Dehydrogenation of Formic Acid. *ACS Catal.* **2015**, *5*, 7099-7103.

(27) He, J.; Waggoner, N. W.; Dunning, S. G.; Steiner, A.; Lynch, V. M.; Humphrey, S. M. A PCP Pincer Ligand for Coordination Polymers with Versatile Chemical Reactivity: Selective Activation of $CO_2$ Gas over CO Gas in the Solid State. *Angew. Chem., Int. Ed.* **2016**, *55*, 12351-12355.

(28) Sawano, T.; Lin, Z.; Boures, D.; An, B.; Wang, C.; Lin, W. Metal–Organic Frameworks Stabilize Mono(phosphine)–Metal Complexes for Broad-Scope Catalytic Reactions. *J. Am. Chem. Soc.* **2016**, *138*, 9783-9786.

(29) Goesten, M. G.; Sai Sankar Gupta, K. B.; Ramos-Fernandez, E. V.; Khajavi, H.; Gascon, J.; Kapteijn, F. Chloromethylation as a functionalisation pathway for metal-organic frameworks. *CrystEngComm* **2012**, *14*, 4109-4111.

(30) Morel, F. L.; Ranocchiari, M.; van Bokhoven, J. A. Synthesis and Characterization of Phosphine-Functionalized Metal–Organic Frameworks Based on MOF-5 and MIL-101 Topologies. *Ind. Eng. Chem. Res.* **2014**, *53*, 9120-9127.

(31) Nuñez, A. J.; Chang, M. S.; Ibarra, I. A.; Humphrey, S. M. Tuning the Host–Guest Interactions in a Phosphine Coordination Polymer through Different Types of post-Synthetic Modification. *Inorg. Chem.* **2013**, *53*, 282-288.

(32) Bezrukov, A. A.; Törnroos, K. W.; Dietzel, P. D. C. Modification of Network and Pore Dimensionality in Metal-Organic Frameworks Containing a Secondary Phosphine Functionality. *Cryst. Growth Des.* **2017**, *17*, 3257–3266.

(33) Amengual, R.; Genin, E.; Michelet, V.; Savignac, M.; Genêt, J.-P. Convenient Synthesis of New Anionic Water-Soluble Phosphanes and Applications in Inter- and Intramolecular Heck Reactions. *Adv. Synth. Catal.* **2002**, *344*, 393-398.

(34) Humphrey, S. M.; Allan, P. K.; Oungoulian, S. E.; Ironside, M. S.; Wise, E. R. Metal-organophosphine and metal-organophosphonium frameworks with layered honeycomb-like structures. *Dalton Trans.* **2009**, 2298-2305.

(35) Dyadkin, V.; Pattison, P.; Dmitriev, V.; Chernyshov, D. A new multipurpose diffractometer PILATUS@SNBL. *J. Synchrotron Radiat.* **2016**, *23*, 825-829.

(36) Rigaku (2015). Rigaku Oxford Diffraction, CrysalisPro Software System. Version 1.171.38.41.

(37) Sheldrick, G., M. SHELXT - Integrated space-group and crystal-structure determination. *Acta Crystallogr., Sect. A* **2015**, *71*, 3-8.

(38) Sheldrick, G., M. Crystal structure refinement with SHELXL. *Acta Crystallogr., Sect. C* **2015**, *71*, 3-8.

(39) Norby, P. Hydrothermal Conversion of Zeolites: An in Situ Synchrotron X-ray Powder Diffraction Study. *J. Am. Chem. Soc.* **1997**, *119*, 5215-5221.

(40) Coelho, A. A.; Evans, J.; Evans, I.; Kern, A.; Parsons, S. The TOPAS symbolic computation system. *Powder Diffraction* **2012**, *26*, S22-S25.

(41) Smeets, S.; McCusker, L. B.; Baerlocher, C.; Elomari, S.; Xie, D.; Zones, S. I. Locating Organic Guests in Inorganic Host Materials from X-ray Powder Diffraction Data. *J. Am. Chem. Soc.* **2016**, *138*, 7099-7106.

(42) Inagaki, M.; Sunahara, M. Gas Adsorption-Desorption Behavior of Activated Carbon Spheres Derived from Phenol Resin. *TANSO* **1998**, *1998*, 146-150.

(43) Simon, C. M.; Smit, B.; Haranczyk, M. pyIAST: Ideal adsorbed solution theory (IAST) Python package. *Comput. Phys. Commun.* **2016**, *200*, 364-380.

(44) Li, J.-R.; Ma, Y.; McCarthy, M. C.; Sculley, J.; Yu, J.; Jeong, H.-K.; Balbuena, P. B.; Zhou, H.-C. Carbon dioxide capture-related gas adsorption and separation in metal-organic frameworks. *Coord. Chem. Rev.* **2011**, *255*, 1791-1823.

(45) Brandys, M.-C.; Puddephatt, R. J. Strongly Luminescent Three-Coordinate Gold(I) Polymers: 1D Chain-Link Fence and 2D Chickenwire Structures. *J. Am. Chem. Soc.* **2001**, *123*, 4839-4840.

(46) Brandys, M.-C.; Puddephatt, R. J. Polymeric Complexes of Silver(I) with Diphosphine Ligands: Self-Assembly of a Puckered Sheet Network Structure. *J. Am. Chem. Soc.* **2002**, *124*, 3946-3950.

(47) Xu, X.; Nieuwenhuyzen, M.; James, S. L. A Nanoporous Metal–Organic Framework Based on Bulky Phosphane Ligands. *Angew. Chem., Int. Ed.* **2002**, *41*, 764-767.

(48) Catalano, V. J.; Malwitz, M. A.; Horner, S. J.; Vasquez, J. Three- and Four-Coordinate Gold(I) Complexes of 3,6-Bis(diphenylphosphino)pyridazine: Monomers, Polymers, and a Metallocryptand Cage. *Inorg. Chem.* **2003**, *42*, 2141-2148.

(49) Tan, X.; Li, L.; Zhang, J.; Han, X.; Jiang, L.; Li, F.; Su, C.-Y. Three-Dimensional Phosphine Metal–Organic Frameworks Assembled from Cu (I) and Pyridyl Diphosphine. *Chem. Mater.* **2012**, *24*, 480-485.

(50) Zhang, S.; Zhang, Z.; Cao, R. Two- and three-dimensional silver acetylide frameworks with high-nuclearity silver cluster building blocks assembled using a bifunctional (4-ethynylphenyl)diphenyl phosphine ligand. *Inorg. Chim. Acta* **2017**, *461*, 57-63.

(51) Yang, Y.-Y.; Lin, Z.-J.; Liang, J.; Huang, Y.; Cao, R. Coordination polymers constructed from a tripodal phosphoryl carboxylate ligand: synthesis, structures and physical properties. *CrystEngComm* **2015**, *17*, 4547-4553.

(52) Spek, A. Structure validation in chemical crystallography. *Acta Crystallogr., Sect. D* **2009**, *65*, 148-155.

(53) Park, H. J.; Lim, D.-W.; Yang, W. S.; Oh, T.-R.; Suh, M. P. A Highly Porous Metal–Organic Framework: Structural Transformations of a Guest-Free MOF Depending on Activation Method and Temperature. *Chem. - Eur. J.* **2011**, *17*, 7251-7260.

(54) He, Y.-P.; Tan, Y.-X.; Wang, F.; Zhang, J. Microporous Zinc Tris[(4-carboxyl)phenylduryl]amine Framework with an Unusual Topological Net for Gas Storage and Separation. *Inorg. Chem.* **2012**, *51*, 1995-1997.

(55) He, Y.-P.; Tan, Y.-X.; Zhang, J. Comparative Study of Activation Methods on Tuning Gas Sorption Properties of a Metal–Organic Framework with Nanosized Ligands. *Inorg. Chem.* **2012**, *51*, 11232-11234.

(56) Shi, D.; Ren, Y.; Jiang, H.; Cai, B.; Lu, J. Synthesis, Structures, and Properties of Two Three-Dimensional Metal–Organic Frameworks, Based on Concurrent Ligand Extension. *Inorg. Chem.* **2012**, *51*, 6498-6506.

(57) Tan, Y.-X.; He, Y.-P.; Zhang, J. Microporous Metal–Organic Framework Based on Mixing Nanosized Tris((4-carboxyl)-phenylduryl)amine and 4,4′-Bipyridine Ligands for Gas Storage and Separation. *Cryst. Growth Des.* **2012**, *12*, 2468-2471.

(58) He, Y.-P.; Tan, Y.-X.; Zhang, J. Gas Sorption, Second-Order Nonlinear Optics, and Luminescence Properties of a Series of Lanthanide–Organic Frameworks Based on Nanosized Tris((4-carboxyl)phenylduryl)amine Ligand. *Inorg. Chem.* **2013**, *52*, 12758-12762.

(59) He, Y.-P.; Tan, Y.-X.; Zhang, J. Stable Mg-Metal–Organic Framework (MOF) and Unstable Zn-MOF Based on Nanosized Tris((4-carboxyl)phenylduryl)amine Ligand. *Cryst. Growth Des.* **2013**, *13*, 6-9.

(60) He, Y.-P.; Tan, Y.-X.; Zhang, J. Guest inducing fluorescence switching in lanthanide-tris((4-carboxyl)phenylduryl)amine frameworks integrating porosity and flexibility. *J. Mater. Chem. C* **2014**, *2*, 4436-4441.

(61) De, D.; Neogi, S.; Sañudo, E. C.; Bharadwaj, P. K. Single-Crystal to Single-Crystal Linker Substitution, Linker Place Exchange, and Transmetalation Reactions in Interpenetrated Pillared–Bilayer Zinc(II) Metal–Organic Frameworks. *Chem. - Eur. J.* **2015**, *21*, 17422-17429.

(62) He, Y.-P.; Tan, Y.-X.; Zhang, J. Gas Sorption, Second-Order Nonlinear Optics, and Luminescence Properties of a Multifunctional srs-Type Metal–Organic Framework Built by Tris(4-carboxylphenylduryl)amine. *Inorg. Chem.* **2015**, *54*, 6653-6656.

(63) De, D.; Neogi, S.; Bharadwaj, P. K. Stoichiometry Controlled Structural Variation in Three-Dimensional Zn(II)–Frameworks: Single-Crystal to Single-Crystal Transmetalation and Selective $CO_2$ Adsorption. *Cryst. Growth Des.* **2016**, *16*, 5238-5246.

(64) Muller, P.; Grunker, R.; Bon, V.; Pfeffermann, M.; Senkovska, I.; Weiss, M. S.; Feng, X.; Kaskel, S. Topological control of 3,4-connected frameworks based on the $Cu_2$-paddle-wheel node: tbo or pto, and why? *CrystEngComm* **2016**, *18*, 8164-8171.

(65) Yao, Q.; Fan, Y.; Wang, Z.; Duan, W.; Wang, S.; Li, Y.; Li, D.; Zhang, Q.; Du, Y.; Dou, J. Coexistence of self- and interpenetration in two (3,6)-connected porous coordination polymers. *CrystEngComm* **2016**, *18*, 8574-8577.

(66) He, Y.-P.; Yuan, L.-B.; Xu, H.; Zhang, J. Control of Interpenetration and Gas-Sorption Properties of Three Mn(II)-tris((4-carboxyl)phenylduryl)amine Frameworks by Tuning Solvent and Temperature. *Cryst. Growth Des.* **2017**, *17*, 290-294.

(67) Liu, Y.; Xuan, W.; Zhang, H.; Cui, Y. Chirality- and Threefold-Symmetry-Directed Assembly of Homochiral Octupolar Metal−Organoboron Frameworks. *Inorg. Chem.* **2009**, *48*, 10018-10023.

(68) Blight, B. A.; Guillet-Nicolas, R.; Kleitz, F.; Wang, R.-Y.; Wang, S. Luminescent Triarylboron-Functionalized Zinc Carboxylate Metal–Organic Framework. *Inorg. Chem.* **2013**, *52*, 1673-1675.

(69) Ma, H.; Sun, D.; Zhang, L.; Wang, R.; Blatov, V. A.; Guo, J.; Sun, D. A. "Strongly" Self-Catenated Metal–Organic Framework with the Highest Topological Density among 3,4-Coordinated Nets. *Inorg. Chem.* **2013**, *52*, 10732-10734.

(70) Kitagawa, S.; Kitaura, R.; Noro, S.-i. Functional Porous Coordination Polymers. *Angew. Chem., Int. Ed.* **2004**, *43*, 2334-2375.

(71) Caskey, S. R.; Wong-Foy, A. G.; Matzger, A. J. Dramatic Tuning of Carbon Dioxide Uptake via Metal Substitution in a Coordination Polymer with Cylindrical Pores. *J. Am. Chem. Soc.* **2008**, *130*, 10870-10871.

(72) Llewellyn, P. L.; Bourrelly, S.; Serre, C.; Vimont, A.; Daturi, M.; Hamon, L.; De Weireld, G.; Chang, J.-S.; Hong, D.-Y.; Kyu Hwang, Y.; Hwa Jhung, S.; Férey, G. High Uptakes of $CO_2$ and $CH_4$ in Mesoporous Metal—Organic Frameworks MIL-100 and MIL-101. *Langmuir* **2008**, *24*, 7245-7250.

(73) Dietzel, P. D. C.; Besikiotis, V.; Blom, R. Application of metal-organic frameworks with coordinatively unsaturated metal sites in storage and separation of methane and carbon dioxide. *J. Mater. Chem.* **2009**, *19*, 7362-7370.

(74) Jayaramulu, K.; Kanoo, P.; George, S. J.; Maji, T. K. Tunable emission from a porous metal-organic framework by employing an excited-state intramolecular proton transfer responsive ligand. *Chem. Commun.* **2010**, *46*, 7906-7908.

(75) Hou, L.; Shi, W.-J.; Wang, Y.-Y.; Guo, Y.; Jin, C.; Shi, Q.-Z. A rod packing microporous metal-organic framework: unprecedented ukv topology, high sorption selectivity and affinity for $CO_2$. *Chem. Commun.* **2011**, *47*, 5464-5466.

(76) Kim, T. K.; Suh, M. P. Selective $CO_2$ adsorption in a flexible non-interpenetrated metal-organic framework. *Chem. Commun.* **2011**, *47*, 4258-4260.

(77) Yu, D.; Yazaydin, A. O.; Lane, J. R.; Dietzel, P. D. C.; Snurr, R. Q. A combined experimental and quantum chemical study of $CO_2$ adsorption in the metal-organic framework CPO-27 with different metals. *Chem. Sci.* **2013**, *4*, 3544-3556.

(78) Das, A.; D'Alessandro, D. M. Tuning the functional sites in metal-organic frameworks to modulate $CO_2$ heats of adsorption. *CrystEngComm* **2015**, *17*, 706-718.

(79) Couck, S.; Denayer, J. F. M.; Baron, G. V.; Rémy, T.; Gascon, J.; Kapteijn, F. An Amine-Functionalized MIL-53 Metal−Organic Framework with Large Separation Power for $CO_2$ and $CH_4$. *J. Am. Chem. Soc.* **2009**, *131*, 6326-6327.

(80) Demessence, A.; D'Alessandro, D. M.; Foo, M. L.; Long, J. R. Strong $CO_2$ Binding in a Water-Stable, Triazolate-Bridged Metal−Organic Framework Functionalized with Ethylenediamine. *J. Am. Chem. Soc.* **2009**, *131*, 8784-8786.

(81) Vaidhyanathan, R.; Iremonger, S. S.; Dawson, K. W.; Shimizu, G. K. H. An amine-functionalized metal organic framework for preferential $CO_2$ adsorption at low pressures. *Chem. Commun.* **2009**, 5230-5232.

(82) An, J.; Geib, S. J.; Rosi, N. L. High and Selective $CO_2$ Uptake in a Cobalt Adeninate Metal−Organic Framework Exhibiting Pyrimidine- and Amino-Decorated Pores. *J. Am. Chem. Soc.* **2010**, *132*, 38-39.

(83) Si, X.; Jiao, C.; Li, F.; Zhang, J.; Wang, S.; Liu, S.; Li, Z.; Sun, L.; Xu, F.; Gabelica, Z.; Schick, C. High and selective $CO_2$ uptake, $H_2$ storage and methanol sensing on the amine-decorated 12-connected MOF CAU-1. *Energy Environ. Sci.* **2011**, *4*, 4522-4527.

(84) Yang, Q.; Wiersum, A. D.; Llewellyn, P. L.; Guillerm, V.; Serre, C.; Maurin, G. Functionalizing porous zirconium terephthalate UiO-66(Zr) for natural gas upgrading: a computational exploration. *Chem. Commun.* **2011**, *47*, 9603-9605.

(85) Liao, P.-Q.; Zhou, D.-D.; Zhu, A.-X.; Jiang, L.; Lin, R.-B.; Zhang, J.-P.; Chen, X.-M. Strong and Dynamic $CO_2$ Sorption in a Flexible Porous Framework Possessing Guest Chelating Claws. *J. Am. Chem. Soc.* **2012**, *134*, 17380-17383.

(86) McDonald, T. M.; Lee, W. R.; Mason, J. A.; Wiers, B. M.; Hong, C. S.; Long, J. R. Capture of Carbon Dioxide from Air and Flue Gas in the Alkylamine-Appended Metal–Organic Framework mmen-$Mg_2$(dobpdc). *J. Am. Chem. Soc.* **2012**, *134*, 7056-7065.

(87) Du, L.; Lu, Z.; Zheng, K.; Wang, J.; Zheng, X.; Pan, Y.; You, X.; Bai, J. Fine-Tuning Pore Size by Shifting Coordination Sites of Ligands and Surface Polarization of Metal–Organic Frameworks To Sharply Enhance the Selectivity for $CO_2$. *J. Am. Chem. Soc.* **2013**, *135*, 562-565.

(88) Liu, B.; Hou, L.; Wu, W.-P.; Dou, A.-N.; Wang, Y.-Y. Highly selective luminescence sensing for $Cu^{2+}$ ions and selective $CO_2$ capture in a doubly interpenetrated MOF with Lewis basic pyridyl sites. *Dalton Trans.* **2015**, *44*, 4423-4427.

(89) Myers, A. L.; Prausnitz, J. M. Thermodynamics of mixed-gas adsorption. *AlChE J.* **1965**, *11*, 121-127.

(90) Zhang, Z.; Zhao, Y.; Gong, Q.; Li, Z.; Li, J. MOFs for $CO_2$ capture and separation from flue gas mixtures: the effect of multifunctional sites on their adsorption capacity and selectivity. *Chem. Commun.* **2013**, *49*, 653-661.

(91) Zhang, Z.; Yao, Z.-Z.; Xiang, S.; Chen, B. Perspective of microporous metal-organic frameworks for $CO_2$ capture and separation. *Energy Environ. Sci.* **2014**, *7*, 2868-2899.

(92) Mason, J. A.; Sumida, K.; Herm, Z. R.; Krishna, R.; Long, J. R. Evaluating metal-organic frameworks for post-combustion carbon dioxide capture via temperature swing adsorption. *Energy Environ. Sci.* **2011**, *4*, 3030-3040.

(93) McDonald, T. M.; D'Alessandro, D. M.; Krishna, R.; Long, J. R. Enhanced carbon dioxide capture upon incorporation of N,N'-dimethylethylenediamine in the metal-organic framework CuBTTri. *Chem. Sci.* **2011**, *2*, 2022-2028.

(94) Cmarik, G. E.; Kim, M.; Cohen, S. M.; Walton, K. S. Tuning the Adsorption Properties of UiO-66 via Ligand Functionalization. *Langmuir* **2012**, *28*, 15606-15613.

(95) Li, B.; Zhang, Z.; Li, Y.; Yao, K.; Zhu, Y.; Deng, Z.; Yang, F.; Zhou, X.; Li, G.; Wu, H.; Nijem, N.; Chabal, Y. J.; Lai, Z.; Han, Y.; Shi, Z.; Feng, S.; Li, J. Enhanced Binding Affinity, Remarkable Selectivity, and High Capacity of $CO_2$ by Dual Functionalization of a rht-Type Metal–Organic Framework. *Angew. Chem., Int. Ed.* **2012**, *51*, 1412-1415.

(96) Du, M.; Li, C.-P.; Chen, M.; Ge, Z.-W.; Wang, X.; Wang, L.; Liu, C.-S. Divergent Kinetic and Thermodynamic Hydration of a Porous Cu(II) Coordination Polymer with Exclusive $CO_2$ Sorption Selectivity. *J. Am. Chem. Soc.* **2014**, *136*, 10906-10909.

**For Table of Contents Only**

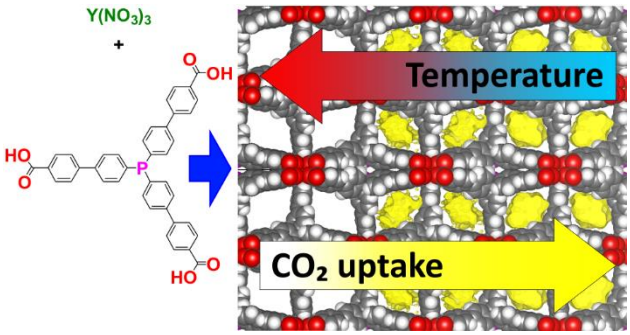


SYNOPSIS

The three-dimensional, non-interpenetrated metal-organic framework [Y(tbpp)]·*n*DMF was synthesized using yttrium(III) and an extended tridentate phosphine linker. The permanently porous material readily adsorbs $N_2$, Ar, $H_2$ and $CO_2$ and it preferentially adsorbs $CO_2$ over $N_2$. A detailed study of the $CO_2$ adsorption process by in-situ powder X-ray diffraction using synchrotron radiation indicates that there are no strong adsorption sites in the channels.